Theor Chem Acc (2013) 132:1342
DOI 10.1007/s00214-013-1342-z

REGULAR ARTICLE

Simulating the optical properties of CdSe clusters using the RT-TDDFT approach

Roger Nadler · Javier Fdez Sanz

Received: 18 October 2012 / Accepted: 15 January 2013 / Published online: 9 February 2013

Abstract The structural and electronic properties of the CdSe nanoclusters, which have been intended to model quantum dots, have been examined by means of time-dependent density functional (TDDFT) calculations. The optical spectra were first simulated using the standard linear response implementation of the TDDFT (LR-TDDFT) in a series of calculations performed using different basis sets and exchange–correlation functionals. In a second step, the real-time TDDFT implementation (RT-TDDFT) was used to simulate the optical absorption spectra of the CdSe nanoclusters, both naked and capped with ligands. In general, we found that the RT-TDDFT approach successfully reproduced the optical spectrum of CdSe clusters offering a good compromise to render both the optical and the geometrical properties of the CdSe clusters at lower computational costs. While for small systems, the standard TDDFT is better suited, for medium- to large-sized systems, the real-time TDDFT becomes competitive and more efficient.

Keywords TDDFT · CdSe · Absorption spectrum · UV–Vis · Quantum dot · Real-time TDDFT

Published as part of the special collection of articles derived from the 8th Congress on Electronic Structure: Principles and Applications (ESPA 2012).

R. Nadler · J. F. Sanz (✉)
Department of Physical Chemistry, University of Seville, 41012 Seville, Spain
e-mail: sanz@us.es

1 Introduction

The flexibility and variety of structures of quantum-confined, semiconducting clusters nowadays opens a vast field of applications. These so-called quantum dots (QDs) can be tuned in size and shape by controlling temperature, solvents, and ligands. For instance, different organic ligand molecules prefer to bind to different facets of a QD, and therefore, the nanocluster will grow along specific directions. Such properties make available the growth of complex nanostructures like tetrapods [1] or hourglass-like nanoclusters [2]. Most certainly, advances in experimental and theoretical methodologies will lead to applications and structures that today just exist in our imagination.

Quantum dots are thought of being artificial atoms since their electronic wave functions are confined in 3 dimensions. This confinement leads to a quantization of the electronic states, resulting in localized orbitals rather than in a band structure description of a bulk semiconductor. The size of a QD is typically within the range of a few nm, which is an order of magnitude smaller than the Bohr exciton radius in the corresponding bulk material. Another consequence of the small size of the QDs is a high surface-to-volume relation, which leads to a particular restructuring of the QD surface. For a CdSe QD, it was shown that the tendency is such that the Cd surface atoms move into the cluster while the Se atoms are puckered out [3, 4]. It is clear that the electronic environment of these surface atoms is different from bulk atoms. Unsaturated bonds occur on the surface, they being a source of surface trap states where electronic charges are trapped. Trap states are responsible for bleaching, that is, when no more excitons can be generated due to the large amounts of energy needed to add another exciton. This process is highly unwanted since excitons formed upon irradiation should be harvested to,

for example, produce electricity in solar cells sensitized with QDs or emit light in a diode. To avoid trap states, these unsaturated bonds, or dangling bonds, need to be passivated.

The QD's popularity comes also from the fact that they possess a high photostability and, most importantly, their absorption spectra can be tuned by simply changing their size. Moreover, the organic capping ligands can easily be replaced by different ligands that could render the QDs water soluble, for instance [5]. This, in turn, offers applications such as bio-labeling material.

Experimentally, there were several attempts to identify the size of CdSe nanoclusters [6–9]. For instance, the cage/core clusters containing 13, 33, and 34 CdSe units were found to be exceptionally stable CdSe clusters by time-of-flight mass spectroscopy [7]. In the smallest of these so-called magic-sized clusters (MSC), the core is formed by one Se atom. A 6-unit cluster just fits nicely inside the $(CdSe)_{28}$ cage which results in a higher binding energy per CdSe unit than for the $(CdSe)_{33}$ cage/core cluster [4]. The first absorption peak of 415 nm (2.98 eV) was attributed to these larger clusters. However, Nguyen et al. [10] found in their calculations that the experimentally observed $(CdSe)_{34}$ cluster is actually the least stable one. Other work used the cluster model consisting of 33 CdSe units [11–16]. Nguyen et al. correlated their result to the fact that the clusters observed by Kasuya et al. by laser ablation experiments might not follow the thermodynamics of $(CdSe)_n$ as they investigated it. Then, Del Ben et al. were able to assign the excitonic transition between 350 and 360 nm (3.44–3.54 eV) to the $(CdSe)_{13}$ cluster by comparing the experimental spectrum obtained by Kudera et al. [8] with that simulated for this specific cluster. Just recently, an experimental paper was published where the authors selectively synthesized $[(CdSe)_{13}(n\text{-octylamine})_{13}]$ and $[(CdSe)_{13}(oleylamine)_{13}]$ nanoclusters [9]. In this paper, the correctness of the assignation was justified by presenting elemental analysis and mass spectroscopy. Also, they used the corresponding spectrum that Del Ben et al. [11] did present for the $(CdSe)_{13}$ QD capped with formate/hydrogen ligand pairs. Both spectra coincide nearly perfectly, even though the two groups used different ligands to obtain their respective spectrum. This is somewhat surprising since Del Ben et al. presented a spectrum for the $(CdSe)_{33}$ cluster that has the dangling bonds saturated with methylamine which is 0.5 eV lower in energy than the QD saturated with the formate/hydrogen ligand pair.

Typically, organic ligand molecules like phosphines, phosphine oxides, thiols, and amines are used to cap the QD, but there are reports that describe the ligation of the QDs with metal-free inorganic ligands like HS^-, S^{2-}, OH^-, and TeS_3^{2-} [17]. Usage of such ligands could increase the efficiency of QDSSC due to a stronger electronic QD–QD coupling [18]. However, it provides the possibility to tune the properties as such as to use QDs as electronic devices, too. Unfortunately, these ligands are not easily incorporated in a model system that could be used for such calculations due to their charged nature.

Albert et al. [15] investigated the dependence of the electronic structure of the $(CdSe)_{33}$ cluster on the computational method and stated that at least a LANL2DZ basis set is necessary to obtain accurate geometries of the clusters. For organic ligands, they propose to also include polarization functions in order to calculate correct binding energies between clusters and ligand molecules. The effect of the exchange–correlation (xc) functional on the lowest-energy optical transitions is more pronounced. Generalized gradient approximation (GGA) functionals underestimate band gaps and miss relevant excitonic effects in the optical transitions, whereas hybrid functionals give results that are more satisfying. On the other hand, they found that solvent effects have only little influence on the absorption spectrum, blue-shifting it by 0.2–0.3 eV. A different study investigated the influence of amines and phosphine oxides on the optical spectrum [12]. They also varied the number of capping ligands in order to observe a change in the spectra. These hybridized surface states near the band gap increase the density of electronic states, the effect being stronger for phosphine oxides than for amines. This behavior suggests a more likely electron–phonon coupling with high-frequency vibrations in the ligand, thus providing a possible explanation of why electron relaxation is more effective when CdSe QDs are capped with phosphine oxides than with amines.

Most commonly, to calculate the electronic spectra to study optical properties of QDs, the linear response time-dependent density functional theory (LR-TDDFT) approach [19] is used [6, 15, 20]. Another methodology is the so-called configuration interaction (CI) [21], applied, for example, in the work of Isborn et al. [22]. The frequency domain or standard implementation of TDDFT and CI is, however, demanding for calculations of medium- and large-sized systems. Recently, it was shown that real-time TDDFT (RT-TDDFT) is a convenient alternative in the computation of the absorption spectra of organic dyes used in solar cells (DSSC) [23–27]. The technique allows for the simulation of not only the dye, but also a relatively well-sized [23–25] cluster representing the semiconducting support. The methodology allows even more elaborate approaches used to calculate the rate of the photoinduced electron transfer [28].

In this paper, we report a computational analysis of the electronic absorption spectra of CdSe QDs by means of RT-TDDFT using a variety of xc-functionals and basis sets available in an all-purpose solid-state chemistry code. In order to facilitate the analysis of the spectra thus obtained,

several spectra have also been computed applying the LR-TDDFT approach. Our aim is to benchmark several xc-functionals and basis sets and to check if and to what extent such technical details influence geometry and optical spectrum of the CdSe quantum dots. After that, we calculated and compared the absorption spectrum of a given nanocluster where different Cd surface atoms were saturated.

2 Models and computational details

Three differently sized CdSe clusters and its ligated variants were employed in this work. The smallest cluster consists of 6 units of CdSe (Fig. 1a, b). It is the smallest possible cluster that still reproduces the wurtzite structure of bulk CdSe. The bond distances d_1 are determined as the Cd–Se bond within the 6-membered ring, whereas d_2 is the bond between a Cd and Se atom located in two adjacent rings. The bond angle α_1 is calculated as the bond angle including Se–Cd–Se, all of them form part of the hexameric ring. Finally, α_2 is the bond angle that includes again Se–Cd–Se but one Se atom is in the other ring. To saturate the Cd atoms, we used 6 molecules of methylamine (MA) (Fig. 1c, d). Yang et al. [29] reported that even for the small $(CdSe)_6$ cluster, the 2-coordinated Cd atoms are not saturated with two ligand molecules; therefore, we will not employ such model systems for ligated clusters. We employed these clusters to simulate the absorption spectra based upon both LR-TDDFT frequency domain calculations and real-time propagation of the wave function in the time domain (RT-TDDFT). Following this procedure, we are able to benchmark the spectra obtained with RT-TDDFT against the LR-TDDFT methodology. Additionally, modeled after the cage/core clusters reported by Kasuya et al. [7], we employed here the $(CdSe)_{13}$ and the $(CdSe)_{34}$ clusters. The medium-sized $(CdSe)_{13}$ cluster consists of a 1 Se atom core as represented in Fig. 2a, b. The saturated cluster, $(CdSe)_{13}(MA)_9$, is sketched in Fig. 2c, d. This is somewhat different to the model employed by Yang et al. [29] where they use 10 ligand molecules. Here, we find that one Cd atom indeed forms bonds to 4 adjacent Se atoms; therefore, we see no need for it to be saturated with a ligand molecule. Finally, the largest cluster, which we have considered for this work, consists of a cage of 28 CdSe units into which a $(CdSe)_6$ core is introduced, cf. Fig. 3a, b. From the 28 surface Cd atoms, six are 4-coordinated. The remaining 22 surface Cd atoms are all 3-coordinated and, consequently, are saturated with one MA molecule (Fig. 3c, d).

From a computational point of view, this work consists of two parts. The first part includes LR-TDDFT calculations, which were performed using the GAUSSIAN 03 program suite [30]. In order to simulate the absorption spectra, over 400 singlet transitions were employed in selected calculations. Four different density functionals and a large number of different basis sets were employed as to investigate the influence of them on the spectra. The basis sets used were LANL2DZ, cc-pVDZ, def2-SVP, and def2-TZVP for both Cd and Se. Effective core potentials (ECP) were employed to describe the core region. For the LANL2DZ basis set, the valence electron density is defined by the $4d^{10}5s^2$ electrons of each Cd and the $4s^2p^4$ electrons for the Se atoms. The valence region described with the cc-pVDZ basis set contains the $4s^2p^6d^{10}5s^2$ electrons for Cd and for Se the $3s^2p^64s^2p^4$ electrons. The def2-SVP and def2-TZVP basis sets include the same valence for Cd as for the cc-pVDZ basis set, while for Se it is an all-electron basis set. When the $(CdSe)_6$ cluster is ligated with methylamine, then the 6-31G(d) basis set was applied to C, N, and H. The xc-functionals were represented by the GGA density functionals PBE [31] and BLYP [32, 33], and two hybrid functionals, PBE0 [34–37] and B3LYP [33, 38]. Since the B3LYP functional was parameterized against the G1 database of Pople et al. [39], for which it gives excellent results, its performance might differ when a system is investigated that contains heavier atoms, as it is the case for semiconductors. It is worth noting that the combination LANL2DZ/B3LYP was reported to reproduce adequately the electronic properties of CdSe systems [40]. The PBE0 hybrid functional, on the other hand, is known to overestimate the band gaps of semiconducting material. The $(CdSe)_6(MA)_6$ system was only calculated with PBE. We did not introduce a solvent model in the calculations as it was shown that the effect on the spectrum is not significant [15].

The second part consists of the calculation of absorption spectra in the time domain using the CP2K/QUICKSTEP program [41, 42], which uses a hybrid Gaussian and plane-wave basis set based on DFT. Here, the PBE and the hybrid PBE0 functionals were considered together with norm-conserving Goedecker–Teter–Hutter (GTH) pseudopotentials [43–45]. For both Cd and Se, the short range, molecularly optimized double-ζ single-polarized basis set (m-SR-DZVP) was applied [46]. For Cd, the $4d^{10}5s^2$ valence electrons are included and for Se the $4s^2p^4$ electrons. It was reported that increasing the basis set for Cd and Se to triple-ζ quality does not result in relevant differences [11]. The m-DZVP basis set is applied on the ligand atoms only. It contains more diffuse functions [46], which is in spirit with Albert et al. [15] who proposed to use polarizable functions at least on the ligand atoms. The geometries were optimized until the gradients were smaller than 0.01 eV/Å and the cutoff for the SCF procedure was set to 10^{-7}. The box length of the simulation cell was set as such that in each direction at least 15 Å of vacuum is

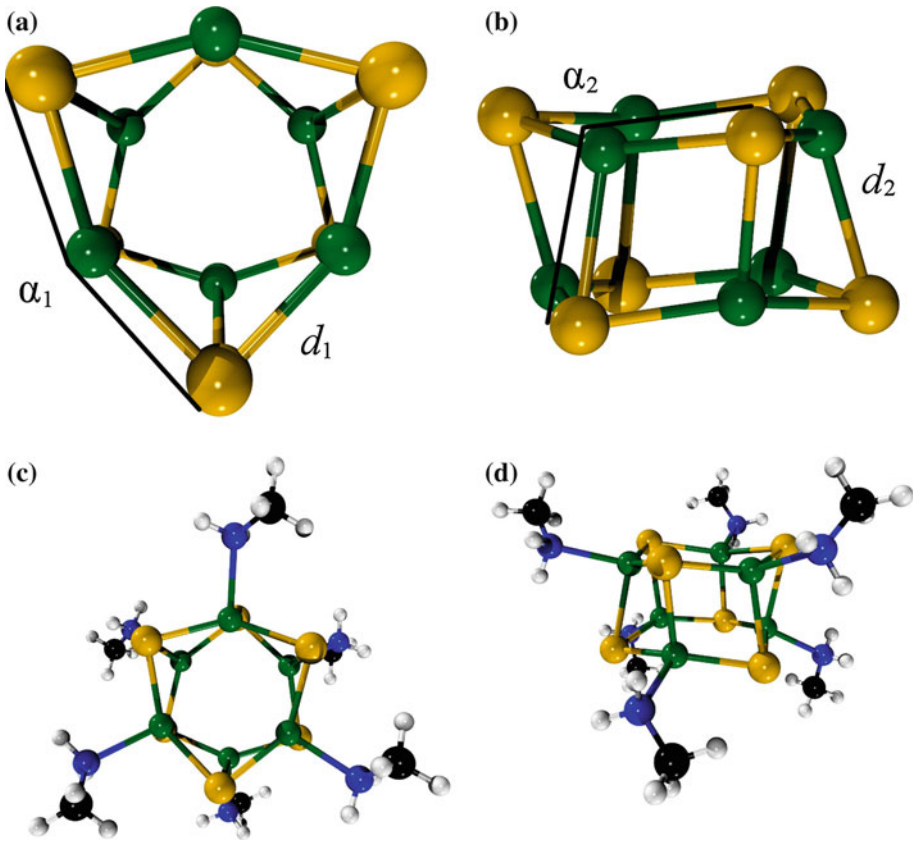

Fig. 1 Sketch of the $(CdSe)_6$ cluster. The *top* view and *side* view of the bare cluster are represented in **a** and **b**, and for the ligated cluster, they are sketched in **c** and **d**. In **a**, the bond distance d_1 and the bond angle α_1 are indicated, whereas in **b**, d_2 and α_2 are shown. See the main text for details. Cd atoms are represented in *green*, Se in *yellow*, N in *blue*, C in *black*, and H in *white*

introduced. The absorption spectra were calculated using the RT-TDDFT methodology introduced by Chen et al. [27]. Shortly, this method consists in applying an ultrashort electromagnetic pulse on the ground-state electronic wave function. It follows the propagation of the perturbed wave function during which the dipole moment for each time step was calculated. Through a Fourier transformation of the induced dipole moment, the absorption cross section will be obtained. Similar to their work, we set a stepwise electric field pulse with duration of 0.0121 fs and a magnitude of 0.5 V/Å. The excited wave function was propagated during 4000 steps, using the ETRS propagator [47], with a time step of 0.0121 fs.

3 Results

First, we look at the geometrical properties of the bare cluster. We observe that the performance of the different basis sets changes. Larger basis sets give better geometries than the smaller ones [15]. In Table 1 are the geometrical parameters tabulated that define the bare cluster. At the B3LYP/LANL2DZ level of theory, the same geometry was reported earlier in literature [6, 10]. The bond lengths obtained with the PBE functional and the m-SR-DZVP basis set almost exactly reproduced the bond lengths obtained when the def2-TZVP basis set is used, indicating a very nice performance of these basis sets in terms of geometrical properties. Again, going along with the findings of Albert et al. [15], we observe that the geometry is quite basis set dependent.

Now, we turn our attention to the optical absorption spectra. In a first step, we quantify the blue-shift induced by saturating the dangling bonds on the Cd atoms by comparing the absorption spectra of $(CdSe)_6$ and the ligated cluster. The spectra computed with the LANL2DZ basis set and the PBE functional, within the LR-TDDFT approach, are represented in Fig. 4. In the bare cluster, the transition occurs at a first absorption peak maximum of 2.68 eV. The excitation takes place between the HOMO-2, which is composed by a large part of 4*p* Se orbitals, and the LUMO, which mainly consists of the 5*s* orbitals on the Cd atoms. This can be rationalized by taking into account the symmetry of the involved MOs. The $(CdSe)_6$ cluster belongs to the D_{3d} point group, and its HOMO-2 has A_{2u} symmetry and its LUMO A_{1g}. The HOMO-1 and the HOMO have E_g symmetry; therefore, the transition between these two MOs and the LUMO is symmetry-forbidden. The first absorption peak maximum for $(CdSe)_6(MA)_6$ is found at 3.08 eV, in very good agreement with the experimental value of 3.14 eV obtained in a TOP/TOPO solvent mixture [6]. The excitonic transition at

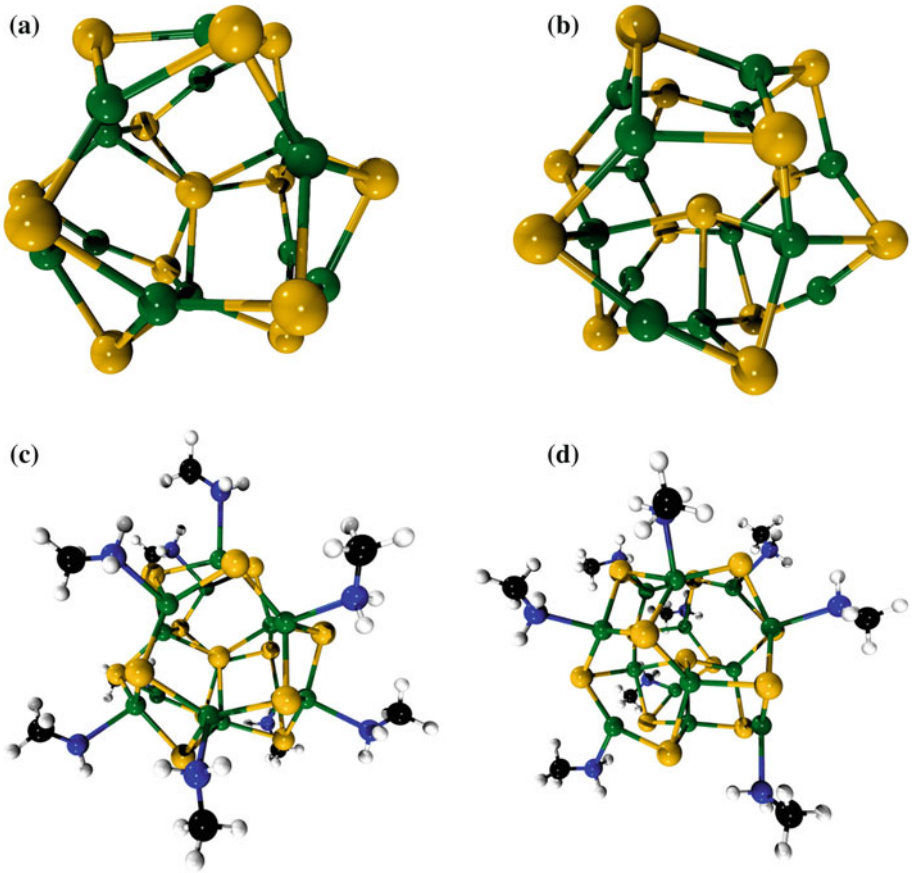

Fig. 2 Sketch of the $(CdSe)_{13}$ cluster. The *top* view and *side* view of the bare cluster are represented in **a** and **b**, and for the ligated cluster, they are sketched in **c** and **d**. There are four 4-coordinated Cd atoms in this cluster. Therefore, only 9 molecules of MA are necessary to saturate the under-coordinated Cd atoms. Cd atoms are represented in *green*, Se in *yellow*, N in *blue*, C in *black*, and H in *white*

3.08 eV includes the HOMO-2, HOMO-1, and HOMO orbitals and excites an electron into the LUMO. The two-fold degeneracy of the HOMO-1 and HOMO must have been broken due to the presence of ligand molecules. We also calculated the spectra for bare cluster where the cc-pVDZ, def2-SVP, and the def2-TZVP basis sets were applied in combination with the PBE functional. We find that these larger basis sets shift the spectrum to the red, which is not desirable in this context.

Let us now compare the spectra obtained with the different xc-functionals. The spectra computed using the LANL2DZ basis set for both Cd and Se are reported in Fig. 5. Clearly, the BLYP functional does not account satisfactorily for the position of the first absorption maximum; it underestimates it by roughly 0.6 eV. On the other extreme, the PBE0 hybrid functional does suffer from its known limitations: it overestimates the first absorption peak by almost 0.4 eV. The B3LYP functional performs much better as it gives a value that is only slightly below the PBE/LANL2DZ result, the difference being as small as 0.06 eV.

We now compare the spectra obtained with RT-TDDFT to the ones simulated with LR-TDDFT methodology. The spectra for the bare and ligated $(CdSe)_6$ clusters are plotted in the top panel of Fig. 6. Compared to the PBE/LANL2DZ spectra of the bare cluster, we observe a red shift of 0.3 eV. This energy is equivalent to a difference of 0.6 eV compared to literature values [4, 22]. When the dangling bonds on Cd are saturated, the performance is slightly better but the energy of the first peak is still underestimated by $\sim$0.14 eV compared to the experimental value [6], and 0.08 eV below the PBE/LANL2DZ value. We think that this is an acceptable deviation since this method allows for the simulation of much larger systems for which LR-TDDFT would be too cumbersome. The blue-shift when the $(CdSe)_6$ is completely ligated, compared to the bare cluster, is found to be 0.6 eV. Surprisingly, the band edge absorption for the bare $(CdSe)_6$ and $(CdSe)_{13}$ clusters nearly coincides. In principle, the band edge for the bare $(CdSe)_{13}$ cluster should be red-shifted due to its larger diameter. For the fully saturated $(CdSe)_{13}(MA)_9$ cluster, the expected red shift is observed again, it being 0.5 eV. For the largest bare cluster $(CdSe)_{34}$, represented in Fig. 3, the first absorption peak is located at 1.86 eV which agrees quite well with results reported earlier in literature [11, 15], the differences being of only 0.1 eV. It should be noted that the herein presented values are not shifted by the difference between the band gap of the bulk material and the theoretical band gap as it was done in Ref. [11]. Our spectrum of the $(CdSe)_{34}$ cluster

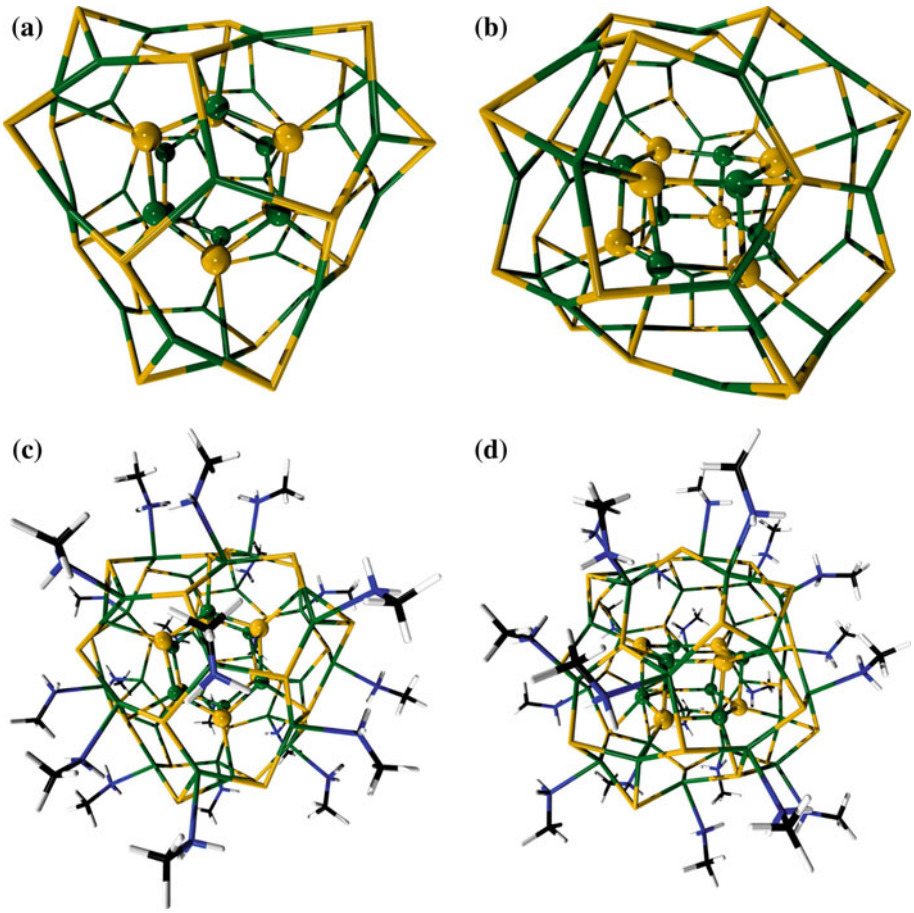

Fig. 3 Illustration of the $(CdSe)_{34}$ cluster. The *top* view and *side* view of the bare cluster are represented in **a** and **b**, and for the ligated cluster, they are sketched in **c** and **d**. Each Se atom of the $(CdSe)_6$ core forms one bond with a Cd atom in the cage. This leads to six 4-coordinated Cd surface atoms, and therefore, 28 MA molecules bound to the remaining under-coordinated Cd atoms. Cd atoms are represented in *green*, Se in *yellow*, N in *blue*, C in *black*, and H in *white*

Table 1 Bond lengths, bond angles, and optical band gaps for the bare $(CdSe)_6$ cluster

	d_1	d_2	α_1	α_2	E_{abs}
PBE, LANL2DZ	2.71	2.87	141.0	100.8	2.68
PBE0, LANL2DZ	2.66	2.82	140.7	100.7	3.03
BLYP, LANL2DZ	2.75	2.91	139.9	100.5	2.08
B3LYP, LANL2DZ	2.70	2.86	139.9	100.4	2.63
PBE, cc-pVDZ	2.60	2.83	145.7	100.7	2.03
PBE0, cc-pVDZ	2.58	2.79	144.6	100.6	–
PBE, def2-SVP	2.61	2.83	145.3	100.4	2.12
PBE, def2-TZVP	2.60	2.83	145.4	100.5	2.11
PBE, m-SR-DZVP	2.61	2.83	145.3	100.3	2.38
PBE0, m-SR-DZVP	2.56	2.80	145.9	100.2	3.41

The distances d_1 and d_2 and the angles α_1 and α_2 are defined in Fig. 1. Distances are in (Å), angles in (°), and the first absorption maximum, E_{abs}, in (eV)

nicely reproduces the one obtained by Del Ben et al. in that their spectrum of the bare $(CdSe)_{33}$ cluster also shows two peaks next to the first absorption peak, located at 1.76 eV, at 1.96 and 2.09 eV (these values are obtained by subtracting 0.43 eV from their results). This is nearly identical to the triple peak in the lowest panel shown in Fig. 6, which shows up at slightly higher energies: 1.86, 2.02, and 2.16 eV, respectively. However, the second peak here is the most intense out of the three peaks while in Ref. [11] it is the least intense one. This could be explained by the orientation of the ligands. Depending on their orientation, the symmetry of the cluster's MOs would be broken in a way that favors a given transition while a different orientation of ligands will favor a different one.

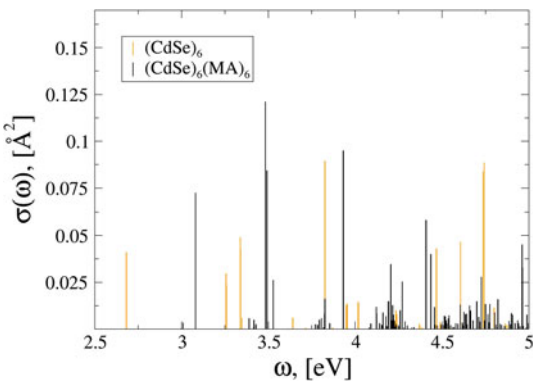

Fig. 4 Optical absorption spectra obtained for the $(CdSe)_6$ and $(CdSe)_6(MA)_6$ clusters. *Yellow lines* correspond to the bare cluster's spectrum, and *black lines* to the caped cluster

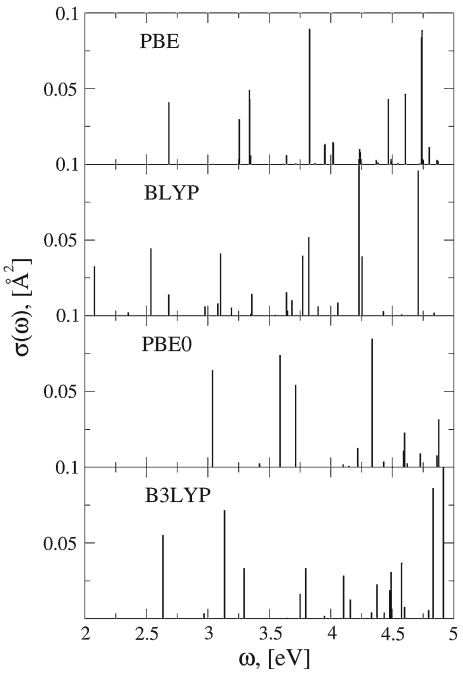

Fig. 5 Absorption spectra of the bare $(CdSe)_6$ cluster obtained with different xc-functional as indicated within each *panel*

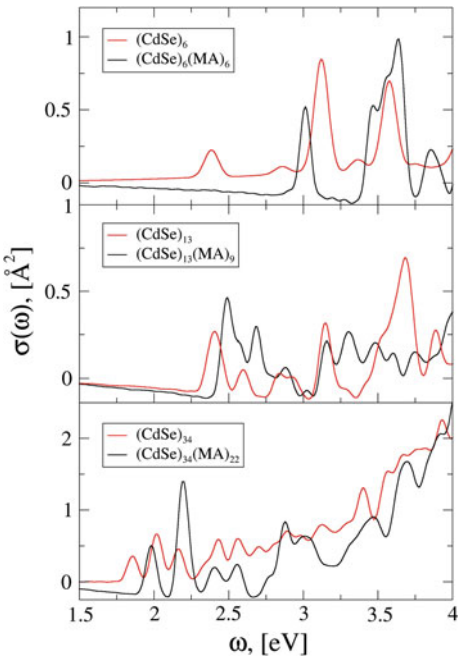

Fig. 6 Absorption spectra calculated with the RT-TDDFT methodology. All spectra were obtained using the PBE functional. In the *top panel* are the spectra of the bare and ligated $(CdSe)_6$ cluster plotted. In the *middle panel*, the corresponding spectra that represent the $(CdSe)_{13}$ and $(CdSe)_{13}(MA)_9$ clusters. In the *lowest panel* are the spectra of $(CdSe)_{34}$ and $(CdSe)_{34}MA_{22}$ plotted. *Red lines* correspond to the bare clusters, and *black lines* to the saturated ones

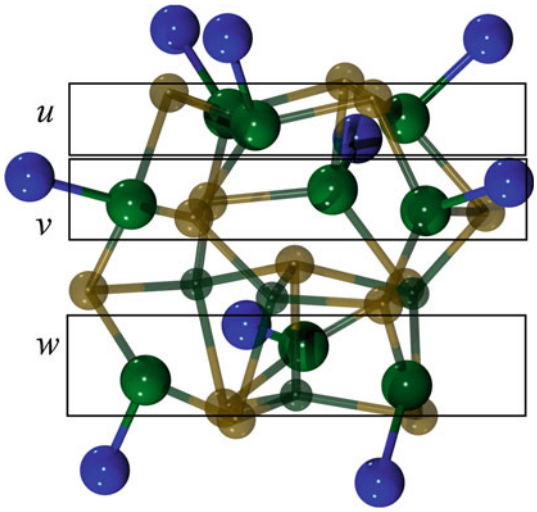

Fig. 7 Represented are the three planes that each consists of 3 Cd atoms that have a similar bonding environment. In plane *u*, the geometry resembles to the 6-membered ring in $(CdSe)_6$. The Cd atoms in plane *v* have a similar bond order than those in plane *u*. Finally, in plane *w*, the Cd atoms are only 2-coordinated

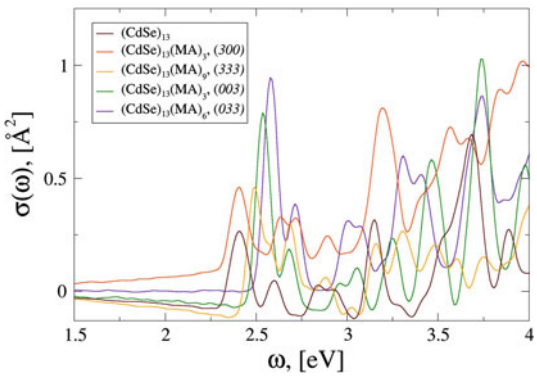

Fig. 8 Illustrated is a series of spectra obtained from the $(CdSe)_{13}$ and $(CdSe)_{13}(MA)_n$ clusters, each having different Cd surface atoms saturated. See the main text for details. The spectra are ordered in ascending order with respect to the first absorption peak

For the saturated $(CdSe)_{34}(MA)_{22}$ cluster, we find $E_{abs} = 1.98$ eV, an underestimation compared to theoretical literature values by approximately 0.16 eV [11] and 1.0 eV when compared to experiment where the CdSe clusters are dissolved in toluene [7]. From this discussion, the disadvantage of the RT-TDDFT methodology emerges. It is very difficult to assign the absorption features in the spectrum and compare them to other experimental and theoretical work because no information about the MOs involved in the excitation is available.

We now analyze the effect of a different number of ligands on the spectrum. The side view in Fig. 7 shows

Table 2 First absorption peak maximum, binding energies of the ligands and bond Cd–N bond lengths for the different ligand/cluster models

	E_{abs}	E_{bind}	d_{Cd-N}, *u*	d_{Cd-N}, *v*	d_{Cd-N}, *w*
(*000*)	2.39	–	–	–	–
(*300*)	2.39	0.50	2.46	–	–
(*333*)	2.49	0.45	2.51	2.50	2.47
(*003*)	2.54	0.60	–	–	2.45
(*033*)	2.58	0.52	–	2.47	2.48
(*030*)	–	0.57	–	2.44	–

The bond lengths are given for each plane as they are defined in Fig. 7. The (*030*) cluster is tabulated for the sake of completeness; no spectrum was calculated for it. E_{abs} and E_{bind} are given both in (eV); all bond lengths are given in (Å)

how the $(CdSe)_{13}$ cluster is divided into three planes *u*, *v*, and *w*, respectively. Each plane consists of 3 Cd atoms that mainly differ in their coordination number. In the planes *u* and *v*, each Cd atom is 3-coordinated while in plane *w* they are only 2-coordinated. The difference between the Cd atoms in plane *u* and *v* is the charge that they carry in the bare cluster which we estimate to be 0.340 *e* in plane *u* and 0.346 *e* in planes *v* and *w* [48]. From these differences, it might be possible that the optical absorption spectrum will be different, too. To investigate the influence of each ligand plane on the absorption spectrum, we modeled in total 4 cluster–ligand systems: $(CdSe)_{13}(MA)_n$ with $n = 3, 6, 9$. We label them in the following manner. The Cd atoms of each plane are saturated with at most three ligands, or they are not saturated at all. We did not consider adding only one or two MAs. Therefore, the fully saturated cluster will be labeled as (*333*), while the bare cluster is labeled (*000*), the labels referring to the planes *u*, *v*, and *w*, respectively. The following cluster–ligand systems were employed: (*003*), (*300*), (*033*), and (*333*), plus the bare cluster: (*000*). The corresponding spectra are plotted in Fig. 8. The plots are ordered with respect to their first absorption maximum feature. Their values are tabulated in Table 2. We observe that the largest blue-shift compared to the bare cluster is induced by the (*033*) model ($E_{abs} = 2.57$ eV), followed by the (*003*) cluster. Between the two extremes, we find the fully saturated cluster, (*333*), with an $E_{abs} = 2.49$ eV. The second $(CdSe)_{13}(MA)_3$ cluster/ligand system, where the *u* plane Cd atoms are saturated, hardly shows a shift in the first absorption peak maximum. Obviously, it is not the (*333*) system that experiences the largest blue-shift but the one where the Cd atoms in the two lowest planes *v* and *w* are saturated, (*033*). Clearly, the impact on the spectrum is largest if the 2-coordinated Cd atoms are saturated, while the influence of saturating 3-coordinated Cd atoms in plane *v* is smaller and it is nearly inexistent when ligands are bound to the *u* plane Cd atoms. The small impact of the *u* plane ligands on the spectrum can be rationalized by analyzing the binding energies of the 3 ligands to the cluster, $E_{bind} = 0.5$ eV, the smallest energy among the systems where only 3 ligands are bound. Yet, the Cd–N bond distance is similar in all three cases. In addition, when no ligands are added, the average charge is not as positive on the *w* plane Cd atoms than on the *u* and *v* plane cadmiums (0.340 *e* vs. 0.346 *e*). For comparison, the average charge is most positive on the 4-coordinated Cd atoms (0.362 *e*). Obviously, the need for saturation of the Cd atoms is smaller in plane *u* than on other surface Cd atoms in the planes *v* and *w*.

When it comes to the PBE0 functional, we find that it overestimates the first absorption peak significantly, both for the $(CdSe)_6$ and the $(CdSe)_{13}$ bare clusters. In the latter, the blue-shift is even more pronounced. While for the smaller QD the difference between the first absorption peaks is 1.0 eV, it increases to 1.3 eV when 13 CdSe units form the QD. Albert et al. [15] reported that one should employ an asymptotically corrected functional like the LC-ωPBE to calculate the energy of the lowest transition closer to experiments.

4 Conclusion

Concerning the geometrical properties of the CdSe clusters, we find that the m-SR-DZVP basis set and the PBE xc-functional give results that are close to results obtained with larger basis sets like def2-TZVP or cc-pVDZ. When the PBE functional is used together with the LANL2DZ basis set, the bond lengths are overestimated compared to the large basis sets.

We also find that the optical properties of CdSe QDs can be successfully reproduced with the RT-TDDFT method using the m-SR-DZVP basis sets and the PBE GGA xc-functional. Therefore, this level of theory offers a good compromise to calculate both geometries and spectra. The PBE0 functional is not recommended for the calculation of optical properties of CdSe clusters since the optical band gap is severely overestimated while B3LYP would be a better choice.

For the $(CdSe)_{13}$ cluster, we find that the absorption spectrum depends on which Cd surface atoms the methylamine ligands are adsorbed to. In particular, when planes *v* and *w* are saturated, the cluster/ligand system shows the strongest blue-shift in the optical spectrum. Moreover, compared to clusters with fewer capping ligands, the fully saturated cluster (9 ligand molecules) shows lower excitation energies.

In summary, the comparison of the conventional LR-TDDFT approach with the less conventional but still already mature RT-TDDFT shows the latter competitive

for large systems, but in contrast, it is not able to give the assignment of the spectral feature. This is an important limitation of RT-TDDFT, which is very stimulating for new theoretical research to overcome or, on the other hand, to improve the LR-TDDFT algorithm in order to become more efficient in large systems but keeping the possibility to give an assignment to the spectral feature, which is a crucial point for the merit of a computational method.

Acknowledgments This work was funded by the Ministerio de Economía y Competitividad (Spain), the EU FEDER program, and the Junta de Andalucía, grants MAT2012-31526, CSD2008-0023, and P08-FQM-3661. Computational resources were provided by the Barcelona Supercomputing Center/Centro Nacional de Supercomputación (Spain).

References

1. Manna L, Milliron DJ, Meisel A, Scher EC, Alivisatos AP (2003) Nat Mater 2:382–385
2. Watt J, Yu C, Chang SLY, Cheong S, Tilley RD (2012) J Am Chem Soc. doi:10.1021/ja311366k
3. Puzder A, Williamson AJ, Gygi F, Galli G (2004) Phys Rev Lett 92:217401–217405
4. Botti S, Marques MAL (2007) Phys Rev B 75:035311–035317
5. Wang J, Xu J, Goodman MD, Chen Y, Cai M, Shinar J, Lin Z (2008) J Mater Chem 18:3270–3274
6. Jose R, Zhanpeisov NU, Fukumura H, Baba Y, Ishikawa M (2006) J Am Chem Soc 128:629–636
7. Kasuya A, Sivamohan R, Barnakov YA, Dmitruk IM, Nirasawa T, Romanyuk VR, Kumar V, Mamykin SV, Tohji K, Jeyadevan B, Shinoda K, Kudo T, Terasaki O, Liu Z, Belosludov RV, Sundararajan V, Kawazoe Y (2004) Nat Mater 3:99–102
8. Kudera S, Zanella M, Giannini C, Rizzo A, Li Y, Gigli G, Cingolani R, Ciccarella G, Spahl W, Parak WJ, Manna L (2007) Adv Mater 19:548–552
9. Wang Y, Liu YH, Zhang Y, Wang F, Kowalski PJ, Rohrs HW, Loomis RA, Gross ML, Buhro WE (2012) Angew Chem Int Ed 51:6154–6157
10. Nguyen KA, Day PN, Pachter R (2010) J Phys Chem C 114:16197–16209
11. Del Ben M, Havenith RWA, Broer R, Stener M (2011) J Phys Chem C 115:16782–16796
12. Kilina S, Ivanov S, Tretiak S (2009) J Am Chem Soc 131(7717): 7726
13. Kilina S, Kilin DS, Prezhdo OV (2009) ACS Nano 3:93–99
14. Kilina S, Velizhanin KA, Ivanov S, Prezhdo OV, Tretiak S (2012) ACS Nano 6:6515–6524
15. Albert VV, Ivanov SA, Tretiak S, Kilina SV (2011) J Phys Chem C 115:15793–15800
16. Abuelela AM, Mohamed TA, Prezhdo OV (2012) J Phys Chem C 116:14674–14681
17. Nag A, Kovalenko MV, Lee JS, Liu W, Spokoyny B, Talapin DV (2011) J Am Chem Soc 133:10612–10620
18. Hillhouse HW, Beard MC (2009) Curr Opin Colloid Interface Sci 14:245–259
19. Casida ME (1996) Recent developments and applications of modern density functional theory. In: Seminario M (ed) Theoretical and computational chemistry, vol 4. Elsevier, Amsterdam, p 391
20. Inerbaev TM, Masunov AE, Khondaker SI, Dobrinescu A, Plamadă AV, Kawazoe Y (2009) J Chem Phys 131:044106–044112
21. Nakatsuji H, Hirao K (1978) J Chem Phys 68:2053–2066
22. Isborn CM, Kilina SV, Li X, Prezhdo OV (2008) J Phys Chem C 112:18291–18294
23. Sánchez-de-Armas R, Oviedo J, San Miguel MA, Sanz JF, Ordejón P, Pruneda M (2010) J Chem Theory Comput 6: 2856–2865
24. Sánchez-de-Armas R, Oviedo J, San Miguel MA, Sanz JF (2011) J Phys Chem C 115:11293–11301
25. Sánchez-de-Armas R, San Miguel MA, Oviedo J, Márquez A, Sanz JF (2011) Phys Chem Chem Phys 13:1506–1514
26. Chen H, Blaber MG, Standridge SD, DeMarco EJ, Hupp JT, Ratner MA, Schatz GC (2012) J Phys Chem C 116:10215–10221
27. Chen H, McMahon JM, Ratner MA, Schatz GC (2010) J Phys Chem C 114:14384–14392
28. Chen H, Ratner MA, Schatz GC (2011) J Phys Chem C 115: 18810–18821
29. Yang P, Tretiak S, Ivanov S (2011) J Clust Sci 22:405–431
30. Frisch MJ, Trucks GW, Schlegel HB, Scuseria GE, Robb MA, Cheeseman JR, Montgomery JA Jr, Vreven T, Kudin KN, Burant JC, Millam JM, Iyengar SS, Tomasi J, Barone V, Mennucci B, Cossi M, Scalmani G, Rega N, Petersson GA, Nakatsuji H, Hada M, Ehara M, Toyota K, Fukuda R, Hasegawa J, Ishida M, Nakajima T, Honda Y, Kitao O, Nakai H, Klene M, Li X, Knox JE, Hratchian HP, Cross JB, Bakken V, Adamo C, Jaramillo J, Gomperts R, Stratmann RE, Yazyev O, Austin AJ, Cammi R, Pomelli C, Ochterski JW, Ayala PY, Morokuma K, Voth GA, Salvador P, Dannenberg JJ, Zakrzewski VG, Dapprich S, Daniels AD, Strain MC, Farkas O, Malick DK, Rabuck AD, Raghavachari K, Foresman JB, Ortiz JV, Cui Q, Baboul AG, Clifford S, Cioslowski J, Stefanov BB, Liu G, Liashenko A, Piskorz P, Komaromi I, Martin RL, Fox DJ, Keith T, Al-Laham MA, Peng CY, Nanayakkara A, Challacombe M, Gill PMW, Johnson B, Chen W, Wong MW, Gonzalez C, Pople JA (2004) Gaussian 03, revision C.02. Gaussian, Inc., Wallingford
31. Perdew JP, Burke K, Ernzerhof M (1996) Phys Rev Lett 77:3865–3868
32. Becke AD (1988) Phys Rev A 38:3098–3100
33. Lee C, Yang W, Parr RG (1988) Phys Rev B 37:785–789
34. Perdew JP, Ernzerhof M, Burke K (1996) J Chem Phys 105:9982–9985
35. Ernzerhof M, Perdew JP, Burke K (1997) Int J Quantum Chem 64:285–295
36. Ernzerhof M, Scuseria GE (1999) J Chem Phys 110:5029–5036
37. Adamo C, Barone V (1999) J Chem Phys 110:6158–6170
38. Becke AD (1993) J Chem Phys 98:5648–5653
39. Pople JA, Head-Gordon M, Fox DJ, Raghavachari K, Curtiss LA (1989) J Chem Phys 90:5622–5630
40. Yang P, Tretiak S, Masunov AE, Ivanov S (2008) J Chem Phys 129:074709–074721
41. The CP2K Developers Group (2000–2013) http://www.cp2k.org
42. VandeVondele J, Krack M, Mohammed F, Parrinello M, Chassaing T, Hutter J (2005) Comput Phys Commun 167:103–128
43. Goedecker S, Teter M, Hutter J (1996) Phys Rev B 54:1703–1710
44. Hartwigsen C, Goedecker S, Hutter J (1998) Phys Rev B 58:3641–3662
45. Krack M (2005) Theor Chem Acc 114:145–152
46. VandeVondele J, Hutter J (2007) J Chem Phys 127:114105–114114
47. Castro A, Marques MAL, Rubio A (2004) J Chem Phys 121: 3425–3433
48. Blöchl PE (1995) J Chem Phys 103:7422–7429